Energy Conversion and Management 200 (2019) 112112

Contents lists available at ScienceDirect

Energy Conversion and Management

journal homepage: www.elsevier.com/locate/enconman

Performance analysis of vaporizer tube with thermoelectric generator applied to cold energy recovery of liquefied natural gas

Minghui Ge[a], Xiaowei Wang[a], Yulong Zhao[a,b,*], Shixue Wang[b], Liansheng Liu[a]

[a] School of Energy and Environmental Engineering, Hebei University of Technology, Tianjin 300401, China
[b] Key Laboratory of Efficient Utilization of Low and Medium Grade Energy (Tianjin University), Ministry of Education, Tianjin 300350,China

ARTICLE INFO

Keywords:
Liquefied natural gas
Cold energy
Thermoelectric
Vaporizer tube
Optimal length

ABSTRACT

The gasification process of liquified natural gas (LNG) releases a significant amount of cold energy. Traditional vaporizers release cold energy directly into the environment, resulting in energy wastage. In this study, a novel type of vaporizer with a thermoelectric generator (VTEG) that combines an air-heated vaporizer and thermoelectric power generation technology is designed. The heat transfer and generation characteristics of the VTEG are analyzed based on the modeling and calculations. The results reveal that compared with the traditional vaporizer, the outer wall temperature of the VTEG increases by 18.4–35.6 K, which mitigates the frosting problem on the surface of the vaporizer. When the fluid is in the liquid-phase and two-phase region, the generation efficiency is maintained between 1.57% and 2.12%. In the gas-phase region, a gradual decrease in the generation efficiency is observed in accordance with an increase in the natural gas temperature. Moreover, the low generation efficiency of the VTEG can be attributed to the low natural convection heat transfer coefficient outside the tube. An increase in tube length first results in an increase in the output power of the VTEG, which then decreases. An optimal tube length exists at which the VTEG output power is maximum value. In addition, the influence of the flow on the single-phase regions is more significant, wherein an approximately linear increase in the optimal tube length and maximum output power occur in accordance with an increase in the flow. Therefore, suitable selection of tube length of the VTEG is very important.

1. Introduction

Given the increase in the severity of environmental problems, natural gas, a type of so-called clean energy, has gradually become one of the most significant energy sources [1]. For long-distance transportation by sea, the natural gas must be cooled to 111 K at atmospheric pressure, thus entering the liquid phase and being transformed into liquefied natural gas (LNG). At this instant, the density increases by a factor of 600 [2]. Low-temperature LNG requires pressurized gasification before it is transported to the user terminal. During the gasification process, approximately 840 MJ of cold energy is released per ton of LNG [3]. The traditional gasification process uses a vaporizer to release the cold energy directly into the sea or air, which results in a waste of energy [4–6].

Several recovery methods exist for LNG cold energy, such as air separation [7], cold storage systems [8], CO_2 capture [9], seawater desalination [10], and power generation [2,11–13]. Among the abovementioned methods, LNG cold energy power generation is one of the most effective methods because of its short industrial chain, in addition to its slight influence from the market, environment, and transportation [14]. LNG cold energy power generation involves the use of low-temperature LNG for the liquefaction of the working medium. The working medium is then heated, gasified, and expanded in the steam turbine to drive the generator. The main approaches are the direct expansion method [15], Organic Rankine cycle (ORC) [16], Kalina cycle [17], Stirling cycle [18], and combined cycle [13]. Although this type of thermodynamic cycle power generation is characterized by high utilization of cold energy, its structure is complex, and its maintenance is challenging. In addition, the high initial investment and the requirement for substantial stable cold capacity restrict its practical application and uptake.

The thermoelectric generator converts thermal energy directly into electrical energy via the thermoelectric effect. Given the absence of chemical reactions and mechanical parts, it offers the advantages of no noise, no pollution, no wear, small size, portability, and extended life span [19–22]. The use of a thermoelectric generator to recover LNG cold energy for power generation is not influenced by the scale of the LNG gasification station and instability of the LNG gasification capacity,

* Corresponding author at: School of Energy and Environmental Engineering, Hebei University of Technology, Tianjin 300401, China.
E-mail address: zhaoyulong12315@163.com (Y. Zhao).

https://doi.org/10.1016/j.enconman.2019.112112
Received 25 June 2019; Received in revised form 21 September 2019; Accepted 25 September 2019
Available online 29 September 2019
0196-8904/

Nomenclature

Symbols

c_p	Specific heat at constant pressure, J/gK
f	Friction coefficient
F	Effective perimeter of finned tube, mm
k	Heat transfer coefficient, W/m^2K^1
l	Length of unit, mm
L	Total length of VTEG, m
m	Mass flow rate, g/s
M	Molar mass
n	Number
p	Pressure, MPa / Price, $
P	Output power, W
q	Heat flux, W/m^2
Q	Quantity of heat, W
r	Radius, mm
T	Temperature, K
t	Time, h
u	Velocity, m/s
U	Design flow, m^3/h
w	Width of PN couple, mm
x	Location in x-axis
X	Dryness
y	Height of fin, mm

Greek symbols

α	Seebeck coefficient, V/K
γ	Latent heat, kJ/kg
δ	Thickness of fin, mm
η	Generation efficiency, %
λ	Thermal conductivity, W/mK
μ	Dynamic viscosity, Pas
ρ	Density, kg/m^3/ Electricity resistance, Ωm
φ	Angle
υ	Kinematic viscosity, m^2/s

Superscripts

i	Unit i

Subscripts

a	Ambient
AL	Aluminum
b	Saturated
ce	Ceramic layer
cu	Copper sheet
e	Electricity
f	Liquid nature gas/ Nature gas
fin	Fin/Inlet fluid
$fout$	Outlet fluid
h	Hot side of PN couple
l	Cold side of PN couple/ liquid-phase
max	Maximum
opt	Optimal
per	Power density
pn	PN couple
r	Circumference/ Contrastive
TE	Thermoelectric module
v	Gas-phase
w	Wall
x	X-axis
1	Inner
2	External

Abbreviations

LNG	Liquefied natural gas
VTEG	Vaporizer tube with thermoelectric generator
ZT	Thermoelectric figure of merit

and has a slight influence on the operation of the original system. Therefore, in several large gasification stations and most small- and medium-sized gasification stations where the use of LNG cold energy is inconvenient, a thermoelectric generator can be flexibly and conveniently employed to generate electricity.

Thermoelectric generators have been widely used in the recovery of waste energy for power generation. Kim et al. [23] used a hexagonal thermoelectric generator to recover the waste heat of exhaust gas for power generation. A generating efficiency of 2.6% was obtained. Zhao et al. [24] proposed an intermediate thermoelectric generator. The simulation results showed that the maximum output power increased by 15.0%, and the corresponding module area decreased by 17.4%. Yin et al. [25] combined a photovoltaic (PV) cell and thermoelectric module to utilize the unwanted heat that may weaken the performance of the PV cell. The result indicated that the total efficiency of the amorphous silicon PV cell increased by approximately 78%. Ge et al. [26] proposed to convert solar energy directly into electricity by using a thermoelectric generator, and pointed out that the cooling system has a greater influence on the net output power of the system. Liu et al. [27] indicated that the use of segmented thermoelectric materials and asymmetrical legs with variable cross-sectional area along the leg length can improve the output power of the solar thermoelectric generator. Zhao et al. [28] applied thermoelectric generation to recover the waste heat of flue gas from a natural gas boiler, and proposed gas humidification to increase the generation capacity of the system. For a geothermal-based organic Rankine cycle, Gholamian et al. [29] used thermoelectric generation to enhance the generation performance of the system.

Thus, the application of thermoelectric generation using normal- and high-temperature waste heat experiments and simulations has been studied in detail [30–33]. However, because of the low ZT value of semiconductor materials at low temperatures and low generation efficiencies, the application of thermoelectric generation in the utilization of LNG cold energy has been limited in low-temperature fields, and only a few relevant studies have been reported. Sun et al. [34] established an analytical solution model for a PN couple. The maximum generation efficiency could reach 9% at the hot and cold side temperatures of 290 K and 130 K, respectively. Karabetoglu et al. [35] developed a single-chip semiconductor thermoelectric generation experimental system, and measured the Seebeck coefficient and resistance of Bi_2Te_3 material in the temperature range of 100–375 K. The results revealed that the maximum output power was achieved at 250 K when the temperature difference was fixed at 200 K. Chung et al. [36] developed a high-performance thermoelectric material that can be used in low-temperature fields, with a ZT value that can reach 0.8 at 225 K. The experimental results of Kambe et al. [37] showed that as the temperature gradient in the direction of module thickness exceeded 200 K/mm, the conventional BiTe thermoelectric modules suffered a sudden decrease in power at cryogenic temperature as low as −160 °C. In addition, the author [38] built an experimental cold energy thermoelectric generation system, and studied the low-temperature generation characteristics of the module using liquid nitrogen as the medium.

Jeong [39] employed a one-dimensional analytic model to study LNG cold energy power generation with a thermoelectric module. The effects of the contact resistance, thermal resistance, and heat transfer capacity at the cold side on the thermoelectric conversion efficiency and optimal external load were analyzed. These aspects were found to have little influence on the generation performance when the contact resistance and contact thermal resistance were lower than 0.0001 Ω and 0.1 K/W, respectively.

In summary, current research on low-temperature thermoelectric generation is focused on the measurement of the physical properties of semiconductor materials at low temperatures and the performance of single thermoelectric module. Research on the thermoelectric device and thermoelectric system that utilizes LNG cold energy is therefore limited, especially with regard to the coupling of complex gasification heat transfer and the thermoelectric conversion of LNG. In this study, a cylindrical thermoelectric vaporizer (VTEG), which combines the air-heated vaporizer with a semiconductor thermoelectric generator and uses the cold energy released from the LNG gasification process to generate electricity, was designed. A mathematical model of the new vaporizer was established, and its effects on the generation characteristics and gasification process were analyzed. The findings of this study can serve as a guide for the design of LNG vaporizers and the performance optimization of LNG cold energy thermoelectric generation.

2. LNG thermoelectric generation vaporizer

2.1. Mathematical model

The traditional air-heated vaporizer is composed of several vertical-finned tube heat exchangers connected in parallel. The traditional vaporizer tube is shown in Fig. 1(a). The LNG is heated by ambient air after its entry into the finned tube from the bottom. The gasification process is completed in three stages: liquid heating, gas-liquid two-phase flow boiling, and gas heating. In this study, a novel type of vaporizer was designed by combining a vaporizer tube with a thermoelectric generator (VTEG), as shown in Fig. 1(b). The VTEG was assembled by the addition of annular thermoelectric modules between the inner heat exchange tube and outer finned tube. Due to the temperature difference between the flowing LNG in the tube and the external environment, the temperature difference between the hot and cold sides of the thermoelectric module can be used for the generation of electrical energy.

In the VTEG, $n_x \times n_r$ thermoelectric modules are electrically connected in series and thermally in parallel, in which n_r thermoelectric modules are arranged along the circumference and n_x thermoelectric modules are arranged in the direction of the tube length. The flow direction along LNG is taken as the x-axis. Along the x direction, the thermoelectric modules in circle i were selected as the research unit to establish the mathematical model, as shown in Fig. 2. The VTEG exchanges heat by natural convection with the air in the environment. Due to heat conduction, heat Q_h^i passes through the outer finned casing tube, outer insulating ceramics, and outer copper sheet, and then

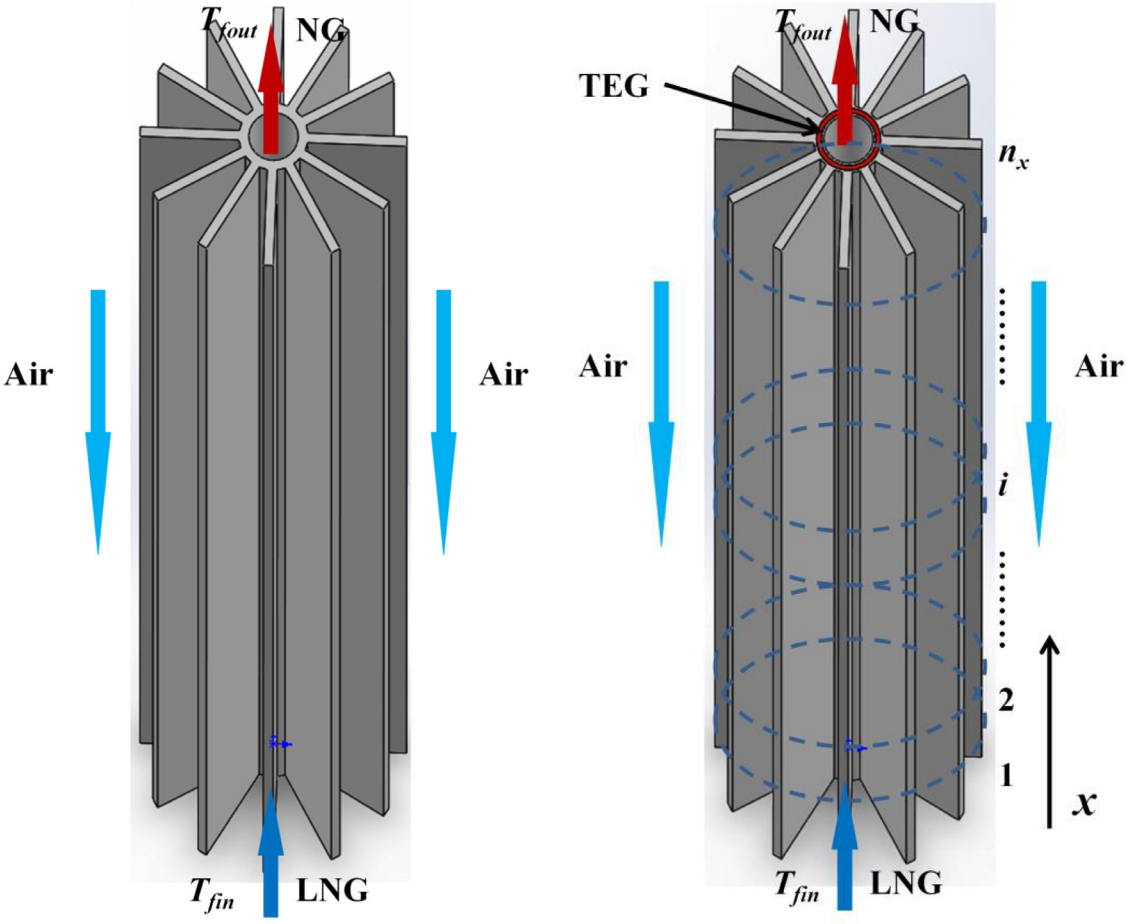

(a) Traditional vaporizer tube (b) Vaporizer tube with thermoelectric generator (VTEG)

Fig. 1. Two types of vaporizer tubes.

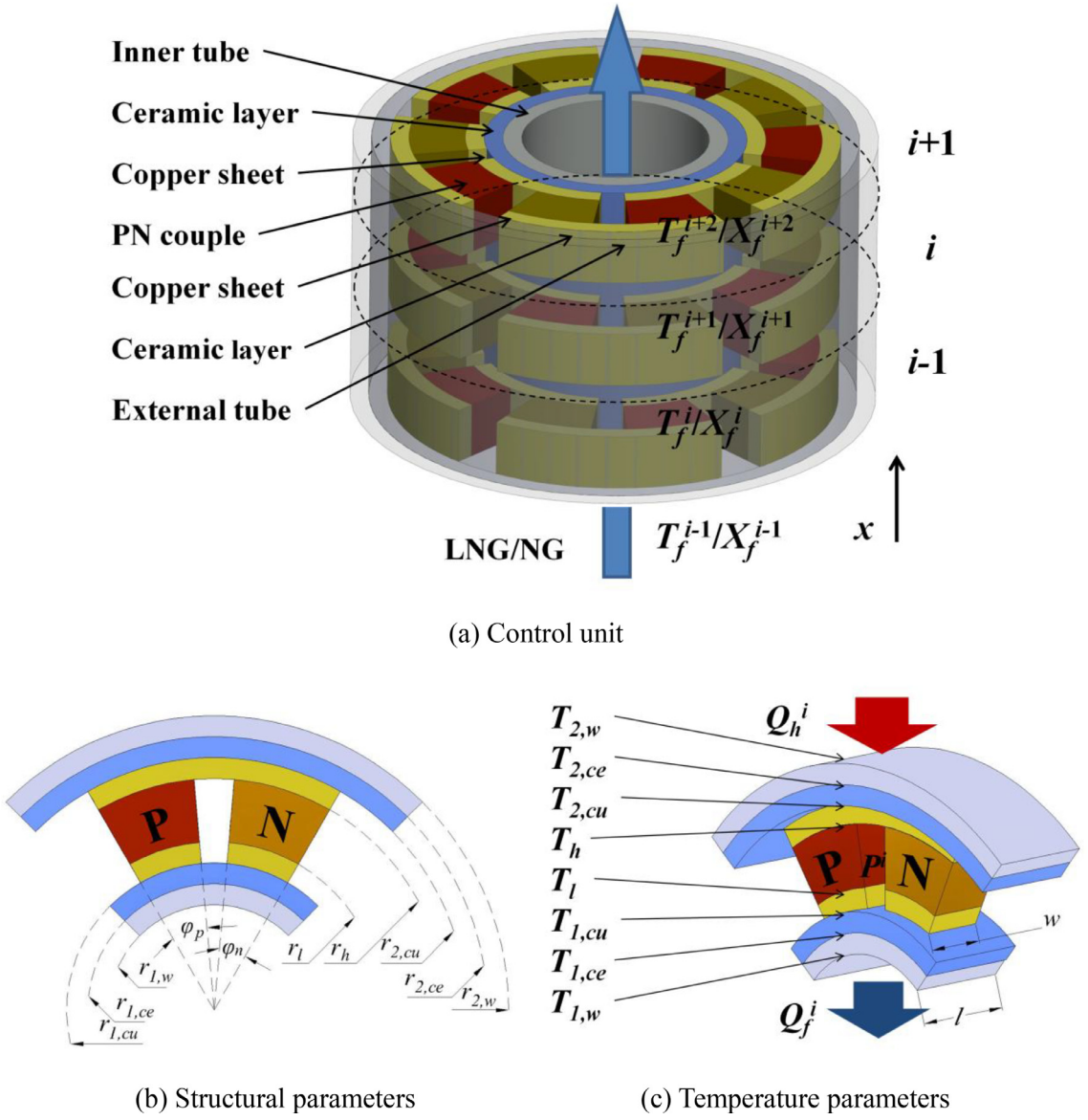

(a) Control unit

(b) Structural parameters

(c) Temperature parameters

Fig. 2. Mathematical model of the VTEG.

reaches the hot side of the PN couple. In the PN couple, a portion of the heat is converted into electrical power P^i, and the remaining energy Q_f^i passes through the inner copper sheet, inner insulating ceramics, and inner casing tube, and then heats the natural gas in the tube, thus resulting in an increase in temperature or gasification. In the circumferential direction, the physical properties of the LNG are considered to remain unchanged, and the n_r thermoelectric modules demonstrate the same power generation performance. Along the direction of the tube length, the generation performances of the modules differ because of the gradual changes in the physical parameters of the fluid, thereby requiring separate calculations.

In the calculation process, the average temperature or dryness of the import and export parameters were taken as the temperature and dryness of the fluid in the control unit, respectively. Considering that the main component of natural gas is methane, this study employed methane instead of natural gas to simplify the calculations. The gasification process was simplified into three sections: the liquid-phase region, two-phase region, and gas-phase region. Moreover, the system was assumed to be in steady state, and the operating pressure was regarded as constant. The sizes of the thermoelectric modules were the same, and the physical parameters of the modules are shown in Table 1. Moreover, axial heat conduction and the Thomason effect were neglected in addition to the contact thermal resistance and contact resistance [40].

2.2. Heat transfer process in the tube

The heat transfer process of natural gas in a tube can be divided into two parts. The process can be considered as single-phase convective heat transfer in the liquid-phase and gas-phase regions. Moreover, in the two-phase region, it can be considered as flow boiling heat transfer. The experimental criterion of forced convective heat transfer can be

Table 1
Physical parameters of the thermoelectric module at $T = 200$ K [34].

Parameters	Unit	Value
Seebeck coefficient of P-type material, α_p	$V K^{-1}$	1.5413×10^{-4}
Seebeck coefficient of N-type material, α_n	$V K^{-1}$	-1.6394×10^{-4}
Electric resistance of P-type material, ρ_p	Ω m	4.1247×10^{-6}
Electric resistance of N-type material, ρ_n	Ω m	5.5236×10^{-6}
Thermal conductivity of P-type material, λ_p	$W m^{-1} K^{-1}$	1.8986
Thermal conductivity of N-type material, λ_n	$W m^{-1} K^{-1}$	1.7796
ZT		0.5702

used to determine when the fluid is in the liquid-phase and gas-phase regions [41].

$$\mathrm{Re}_f^i = \frac{2u_f^i r_{1,w}}{\upsilon_f^i} \tag{1}$$

where Re_f^i is the Reynolds number of the fluid, u_f^i is the flow rate of the fluid, $r_{1,w}$ is the inner radius of the tube, and υ_f^i is the kinematic viscosity of the fluid.

The friction coefficient of the wall f_f^i can be calculated according to Re_f^i [42], as follows:

$$f_f^i = 64/\mathrm{Re}_f^i (\mathrm{Re}_f^i \leqslant 2000) \tag{2}$$

$$f_f^i = 0.316\mathrm{Re}_f^{i-0.25} (2000 \leqslant \mathrm{Re}_f^i \leqslant 20,000) \tag{3}$$

$$f_f^i = 0.184\mathrm{Re}_f^{i-0.2} (\mathrm{Re}_f^i \geqslant 20,000) \tag{4}$$

The conductive heat transfer coefficient in tube k_f^i can be calculated according to the convective heat transfer criterion [41].

$$St_f^i = 0.125 f_f^i \mathrm{Pr}_f^{i-2/3} \tag{5}$$

$$k_f^i = St_f^i \rho_f^i u_f^i c_{p,f}^i \tag{6}$$

where St_f^i is the Stanton number, Pr_f^i is the Prandtl number, ρ_f^i is the density of the fluid, and $c_{p,f}^i$ is the specific heat capacity at constant fluid pressure.

The heat exchange of the fluid in the control unit Q_f^i can be expressed as follows:

$$Q_f^i = m_f c_{p,f}^i (T_f^{i+1} - T_f^i) = k_f^i 2\pi r_{1,w} l \left(T_{1,w}^i - \frac{T_f^i + T_f^{i+1}}{2} \right) \tag{7}$$

where m_f is the mass flow rate of the fluid; T_f^i and T_f^{i+1} are the inlet and outlet temperatures of the fluid in the unit, respectively; l is the height of the unit; and $T_{1,w}^i$ is the inner wall temperature of the control unit.

The heat transfer coefficient of Zou [43] can be used when the fluid is in the flow boiling region.

$$k_f^i = [(E^i k_{sp}^i)^2 + (S^i k_{nb}^i)^2]^{0.5} \tag{8}$$

where

$$k_{sp}^i = 0.023(\mathrm{Re}_l)^{0.8}(\mathrm{Pr}_l)^{0.4}\frac{\lambda_l}{2r_{1,w}} \tag{9}$$

$$\mathrm{Re}_l = \frac{2G_f r_{1,w}}{\mu_l} \tag{10}$$

$$E^i = \left[1 + \frac{X^i + X^{i+1}}{2} \mathrm{Pr}_l (\rho_l/\rho_v - 1) \right]^{0.35} \tag{11}$$

$$k_{nb}^i = 55 p_r^{0.12} (-\log_{10} p_r)^{-0.55} M^{-0.5} q_f^{i0.67} \tag{12}$$

$$S^i = [1 + 0.055(E^i)^{0.1}(\mathrm{Re}_l)^{0.16}]^{-1} \tag{13}$$

where G_f is the mass flow rate of the fluid per unit area; Re_l, Pr_l, ρ_l, λ_l, and μ_l are the Reynolds number, Prandtl number, density, thermal conductivity, and dynamic viscosity of the liquid phase, respectively; ρ_v is the density of the gas phase; M is the molar mass of methane; q_f^i is the heat flux; p_r is the contrastive pressure (ratio of liquid pressure to critical pressure); and X^i and X^{i+1} are the inlet and outlet dryness values of the control unit, respectively.

The heat exchange of the fluid in the control unit can be expressed as follows:

$$Q_f^i = m_f \gamma (X_f^{i+1} - X_f^i) = k_f^i 2\pi r_{1,w} l (T_{1,w}^i - T_b) \tag{14}$$

where γ and T_b are the latent heat and saturated temperature of methane, respectively.

The heat exchange between the fluid and the inner wall of tube Q_f^i passes through the insulating ceramic circle, conductive cooper sheet, and metal casing tube, and then reaches the cold side of the thermoelectric module. The heat transfer process can be expressed as follows:

$$Q_f^i = \frac{2\pi\lambda_{AL} l (T_{1,w}^i - T_{1,ce}^i)}{\ln(r_{1,ce}/r_{1,w})} = \frac{2\pi\lambda_{ce} l (T_{1,ce}^i - T_{1,cu}^i)}{\ln(r_{1,cu}/r_{1,ce})} = \frac{2\pi\lambda_{cu} l (T_{1,cu}^i - T_l^i)}{\ln(r_{1,l}/r_{1,cu})} \tag{15}$$

where λ_{AL}, λ_{ce}, and λ_{cu} are the thermal conductivities of the inner tube, ceramic layer, and conductive copper sheet, respectively; $r_{1,ce}$, $r_{1,cu}$, and $r_{1,l}$ are the radii of the inner ceramic layer, inner ceramic layer, and module, respectively; $T_{1,ce}^i$ and $T_{1,cu}^i$ are the wall temperatures of the inner ceramic and inner conductive copper sheets, respectively; and T_l^i is the cold side temperature of the annular PN couple.

2.3. Thermoelectric conversion process

The energy equations for the annular PN couple can be expressed as follows:

$$Q_h^i = n_r(\alpha_{pn} T_h^i I + K_{pn}(T_h^i - T_l^i) - 0.5 I^2 R_{pn}) \tag{16}$$

$$Q_l^i = n_r(\alpha_{pn} T_l^i I + K_{pn}(T_h^i - T_l^i) + 0.5 I^2 R_{pn}) \tag{17}$$

where Q_h^i is the energy received by the hot side of the PN couple, n_r is the number of PN couples in the circumferential direction, α_{pn} is the Seebeck coefficient of the PN couple, K_{pn} is the thermal conductance of the PN couple, R_{pn} is the electric resistance of the PN couple, T_h^i is the hot side temperature of the PN couple, and I is the electric current in the module.

The thermal conductance K_{pn} and electric resistance R_{pn} can be calculated as follows [44]:

$$K_{pn} = \frac{(\lambda_p \varphi_p + \lambda_n \varphi_n) l}{\ln(r_h/r_l)} \tag{18}$$

$$R_{pn} = \frac{\rho_p \ln(r_h/r_l)}{\varphi_p l} + \frac{\rho_n \ln(r_h/r_l)}{\varphi_n l} \tag{19}$$

where λ_p and λ_n are the thermal conductivities of the P- and N-type materials, respectively; ρ_p and ρ_n are the resistivity of the P- and N-type materials, respectively; r_h and r_l are the outer and inner radii of the curve PN couple, respectively; and φ_p and φ_n are the thermoelectric leg angles of the P- and N-type materials, respectively.

2.4. Heat transfer process outside the tube

The heat is transferred by natural convection between the VTEG and ambient air. The heat transfer equation can be expressed as follows:

$$Q_h^i = k_a^i F l (T_a - T_{2,w}^i) \tag{20}$$

where k_a^i is the natural convection heat transfer coefficient of the outer wall of the tube, F is the effective perimeter of the finned tube, T_a is the ambient temperature, and $T_{2,w}^i$ is the outside wall temperature of the tube.

The natural convection heat transfer outside the tube can be expressed as follows [41]:

$$Nu = \left(0.825 + \frac{0.387 Ra^{1/6}}{[1 + (0.492/\mathrm{Pr})^{9/16}]^{8/27}} \right)^2 \tag{21}$$

$$k_a^i = \frac{Nu\lambda_a^i}{L} \tag{22}$$

where Ra is the Rayleigh number, Pr is the Prandtl number, λ_a^i is the thermal conductivity of air, and L is the length of the VTEG. The average temperature of the wall and the environment is considered as the qualitative temperature of air.

The effective perimeter outside tube F can be obtained using the

following equation:

$$F = 2\pi r_{2,w} + n_{fin}(2y + \delta)\eta_{fin} \tag{23}$$

where $r_{2,w}$ is the external radius of the finned tube, y is the height of the fin, δ is the thickness of the fin, η_{fin} is the efficiency of the fin, and n_{fin} is the number of fins in the circumferential direction.

The efficiency of the fin characterizes the effectiveness of heat dissipation of fin, it can be obtained as follows [41]:

$$\eta_{fin} = \frac{\tanh(my)}{my} \tag{24}$$

$$m = \sqrt{\frac{2k_a^i}{\lambda_{AL}\delta}} \tag{25}$$

where tanh is the hyperbolic tangent, λ_{Al} is the thermal conductivity of the fin.

Due to heat conduction, the heat transfer outside the tube Q_h^i passes through the outer finned tube, ceramics layer, and copper sheet before reaching the hot side of the PN couple. Moreover, it is given by

$$Q_h^i = \frac{2\pi\lambda_{cu}l(T_h^i - T_{2,cu}^i)}{\ln(r_{2,cu}/r_h)} = \frac{2\pi\lambda_{ce}l(T_{2,cu}^i - T_{2,ce}^i)}{\ln(r_{2,ce}/r_{2,cu})} = \frac{2\pi\lambda_{AL}l(T_{2,ce}^i - T_{2,w}^i)}{\ln(r_{2,w}/r_{2,ce})} \tag{26}$$

where $r_{2,cu}$ and $r_{2,ce}$ are the external radii of the outer conductive copper sheet and ceramic layer, respectively; and $T_{2,ce}{}^i$ and $T_{2,cu}{}^i$ are the outer wall temperatures of the outer conductive copper sheet and ceramic layer, respectively.

2.5. Overall performance of the generator tube

The output power P and generation efficiency η of the entire VTEG can be calculated as follows:

$$P = \sum_{i=1}^{n_x} P^i = \sum_{i=1}^{n_x} (Q_h^i - Q_f^i) \tag{27}$$

$$\eta = P / \sum_{i=1}^{n_x} Q_h^i \tag{28}$$

The total length of the VTEG is given by

$$L = n_x l \tag{29}$$

The flow chart of the calculation is shown in Fig. 3. A Matlab computer program was used to perform the calculations. In the calculation, a predicted current value was first assigned for the VTEG, and then, the temperature distribution of all the modules and a new current value I were obtained according to the given tube length L and the operation parameters. If the new current value differed from the predicted value, the latter was corrected and recalculated until the two are equal.

2.6. Calculation parameters

Numerical calculations were carried out for the air-heated vaporizer of a gasification peak shaving station [45]. The designed gasification capacity was 5000 m^3/h, and the operating pressure was 1.6 MPa. The vaporizer consisted of 72 finned tubes, each with an internal diameter of 10 mm, an external diameter of 14 mm, and a length of 13.32 m. Each vaporizer tube had 12 fins. In the actual operation, LNG with a temperature of 112 K flows into each tube from the lower part of the main tube. In each vaporizer tube, the three stages of liquid heating, gas–liquid two-phase flow boiling, and gas heating occur. Finally, the LNG is heated to 263 K and discharged from the upper exit of the finned tube. The structure and operating parameters of the VTEG are shown in Table 2.

2.7. Model validation

To date, experimental study on annular thermoelectric generator has not been reported in the literature. The simulation results in Ref. [46] are compared with the model in this study, and the results are shown in Fig. 4 (a). In Ref. [46], annular thermoelectric modules with different structural parameters were analyzed under the hot and cold side temperatures of 400 K and 300 K. The error between the results of this model and those of Ref. [46] is less than 4%. In addition, the model was validated using the experimental data of a plate thermoelectric generation system [47]. Without considering the effects of contact thermal resistance and contact resistance and using fixed physical parameters for the module in the calculation, the error between the predicted results and the experimental data is less than 10%. However, in general, the proposed model can predict the experimental data well, especially the maximum output power [48].

3. Results and discussion

3.1. Basic characteristics of the proposed generation vaporizer

To analyze the influence of the thermoelectric module on the vaporizer, the results of the comparison between the temperature distribution of the outer wall of the conventional vaporizer and the VTEG are shown in Fig. 5. For the traditional vaporizer, the calculation results

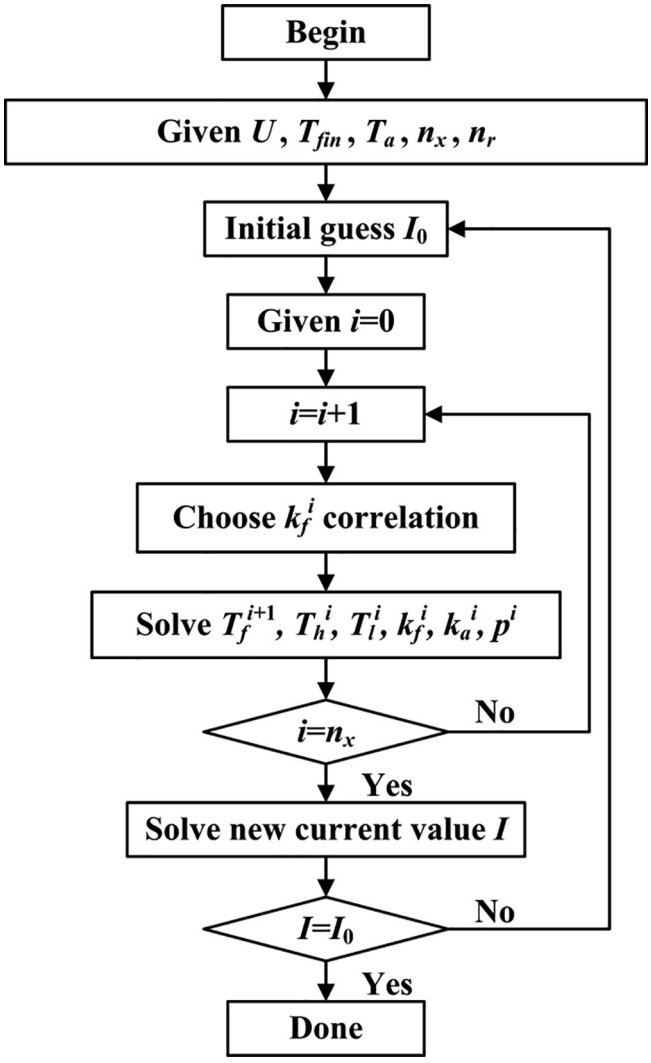

Fig. 3. Flow chart of calculation.

Table 2
Structural and operating parameters of the VTEG.

Parameters	Unit	Value
Structural parameters		
Number of PN couples in circumferential direction, n_r		4
Angle, $\varphi_p = \varphi_n$		2π/15
Length of module, l	mm	5
Inner radius of tube, $r_{1,w}$	mm	5
Radius of inner ceramic tube, $r_{1,ce}$	mm	7
Radius of cold side of module, r_l	mm	7.5
Radius of hot side of module, r_h	mm	9.5
Radius of outer ceramic tube, $r_{2,ce}$	mm	10
Outer radius of tube, $r_{2,w}$	mm	10.5
Height of fin, y	mm	80
Thickness of fin, δ	mm	2
Number of fin, n_f		12
Thermal conductivity of aluminum, λ_{AL}	W/mK	162
Thermal conductivity of aluminum, λ_{ce}	W/mK	25
Operating parameters		
Design total flow, U	m^3/h	5000/72
Operating pressure, p	MPa	1.6
Inlet temperature of LNG, T_{fin}	K	112
Ambient temperature, T_a	K	283

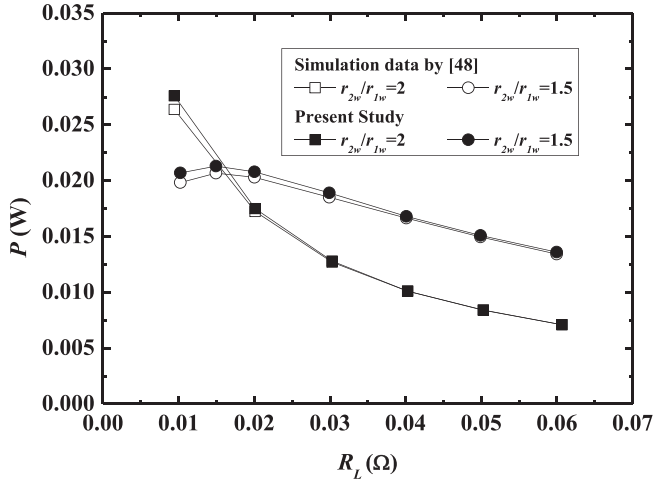

(a) Comparison with numerical results

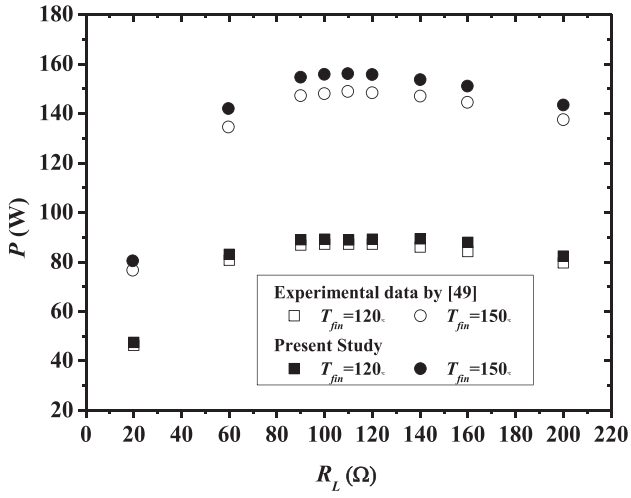

(b) Comparison with experimental results

Fig. 4. Validation of the proposed numerical model.

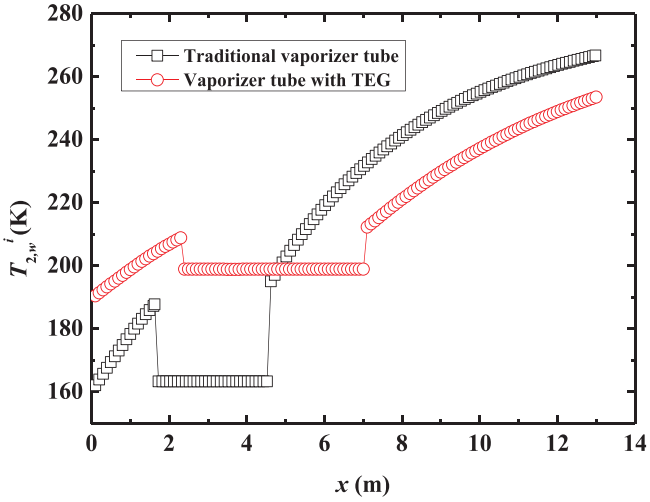

Fig. 5. Comparison of outside wall temperature for the two types of finned tubes.

revealed that the tube length required to complete the gasification process is 12.98 m, which is very close to the length of the actual tube. This verifies the reliability of the heat transfer calculation. In addition, the whole gasification process can be clearly divided into the liquid-phase region, two-phase region, and gas-phase region. Moreover, the tube lengths required at each stage of the gasification process were significantly different. The gas-phase heat transfer region had the greatest length (8.46 m), followed by the two-phase region (2.89 m), and the liquid-phase region (1.63 m). The figure shows that for the traditional vaporizer, the outer wall temperature of the tube was very low. In particular, in the liquid-phase and two-phase regions, the temperature was lower than 190 K. Hence, during the operation of the vaporizer, a thick ice layer will form on the surface, which will cause the deterioration of heat transfer and lower the outlet temperature of the natural gas compared to the design value.

The VTEG with the same length as the traditional fin tube was selected for the calculations. The results revealed that when compared with the traditional fin tube, the heat transfer resistance of the VTEG increased because of the presence of the PN couples and insulating ceramics, and there was a significant increase in the outer wall temperature of tube. In particular, in the liquid-phase and two-phase regions, the wall temperature increased by 18.4–35.6 K. Considering that the lower the outer wall temperature of the tube, the thicker the ice layer [49], the new vaporizer plays an active role in suppressing the frost formation on the wall. Simultaneously, because of the increase in the heat transfer resistance, the outlet temperature of the natural gas of the VTEG was 244 K, which is 19 K lower than that of the traditional vaporizer. This implies that it is necessary to extend the length of the vaporizer to reach the required temperature of the natural gas.

Fig. 6 presents the variation characteristics of the generation density and efficiency of the VTEG (*x*-direction). In the liquid-phase region, a gradual increase in the LNG temperature was accompanied by decreases in the generation efficiency and density. However, the generation efficiency and density were relatively high (i.e., 1.57%–2.12% and 14.3–26.6 W/m, respectively). When entering the two-phase region, the generation efficiency and density increased abruptly to 1.91% and 20.8 W/m, respectively. Moreover, throughout the two-phase region, the changes in the generation efficiency and density were slight. When the fluid was in the gas phase, a further increase in the natural gas temperature resulted in an abrupt decrease in the generation efficiency and density. The output power of the entire tube was 105.8 W, and the average generation efficiency was 1.32%. Fig. 6 also shows that the generation efficiency of the module near the outlet was negative, which implies that this part of the module was a load. This aspect decreased

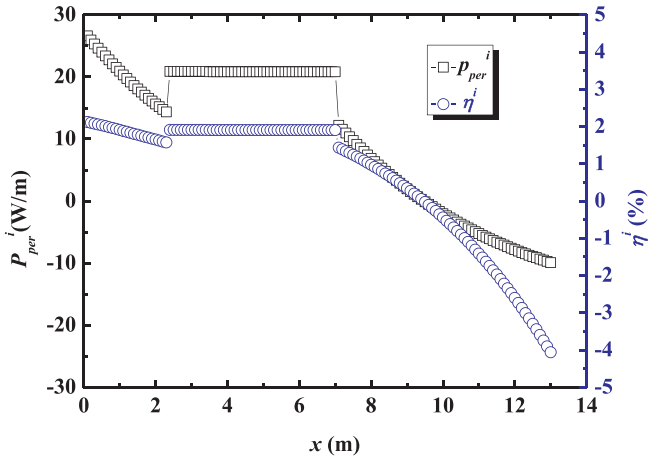

Fig. 6. Variations in power density and power generation efficiency (x-axis).

the output power of the system, resulting in module wastage and lowering the economy of the system. It is therefore necessary to extensively investigate the influence of the VTEG length on the power generation performance.

Fig. 7 presents the temperature distribution (x-axis). The figure shows that although the temperature of the natural gas in the tube was significantly different from that of the outer environment, the temperature difference between the two ends of the PN couple was less than 42 K, which accounted for less than 30% of the total temperature difference (external environment temperature T_a − LNG temperature T_f), as shown in Fig. 7(b). This phenomenon was attributed to the existence of the natural convection heat transfer resistance outside the tube, heat conduction resistance of the tube, and heat transfer resistance within the tube. Therefore, in general, the generation efficiency and density of the fin tube were low. Moreover, the main heat transfer resistance was found to be the natural convection heat transfer outside the tube, which accounted for more than 50% of the heat transfer. In particular, in the two-phase region, the thermal resistance accounted for 68.4% of the total thermal resistance.

Fig. 8 reveals the distribution characteristics of the heat transfer coefficient inside and outside the fin tube. In the liquid-phase region, the convective heat transfer coefficient increased slightly because of the increase in the LNG temperature; however, the actual effective temperature difference $T_h^{\ i} - T_l^{\ i}$ decreased because of the increase in the fluid temperature in the tube (Fig. 7). Upon its entry into the flow boiling region, there was an abrupt increase in the heat transfer coefficient in the tube. At this instant, there was a slight increase in the temperature difference between the hot and cold sides of the PN couple. Thereafter, the fluid in the tube changed phase and the temperature was constant; thus, the change in the effective temperature difference $T_h^{\ i} - T_l^{\ i}$ was slight (Fig. 7), as were the changes in the generation efficiency and density (Fig. 6). In the gas-phase region, although no significant changes occurred in the heat transfer coefficient in the tube, the effective temperature difference $T_h^{\ i} - T_l^{\ i}$ gradually decreased because of the continuous heating of the fluid, which resulted in reductions in the generation efficiency and density. In addition, the figure shows that the natural convection heat transfer coefficient outside the tube was 4.5–7.5 W/m^{2}K; hence, the hot side was at a significantly lower temperature than the ambient temperature. Therefore, further optimization of the fin structure outside the tube can be considered in the follow-up application to improve the heat transfer capacity, and thus the generation efficiency and power generation density. Moreover, considering the high convective heat transfer coefficient of seawater outside the tube, the model in this study can be applied in the seawater vaporizer, which will likely provide better generation performance.

3.2. Maximum output power and optimal tube length

As mentioned above, the VTEG length influences the vaporization process of LNG in addition to the output power of the system, and the latter is directly related to the economy of the VTEG. It is therefore necessary to investigate the influence of the tube length on the VTEG generation characteristics and operation parameters. The results are shown in Fig. 9. As shown in Fig. 9 (a), the output power and generation efficiency curves are clearly divided into three regions. First, with an increase in the tube length, the output power increased gradually with decreasing amplification, and the generation efficiency gradually decreased. At this instant, the outlet temperature of the LNG was lower than the boiling point (i.e., the LNG was in the liquid state). When the tube length exceeded 2.3 m, with a continuous increase in the tube length, the outlet natural gas entered the two-phase region, the output power increased approximately linearly, and the generation density was maintained at 1.8%. When the tube length reached 6.9 m, the outlet fluid was gaseous. The continuous increase in the tube length was accompanied by a gradual increase in the output power; however, there was a clear decrease in the amplification, and the maximum value of 155.2 W was reached at 8.9 m. Thereafter, there was a gradual decrease in the output power and generation efficiency. In addition, it is notable that when the maximum output power was obtained, the outlet LNG temperature was 197.8 K, which did not yet meet the user requirement. Continuous VTEG use is associated with the problems of high cost and low output power. Therefore, the traditional vaporizer can be

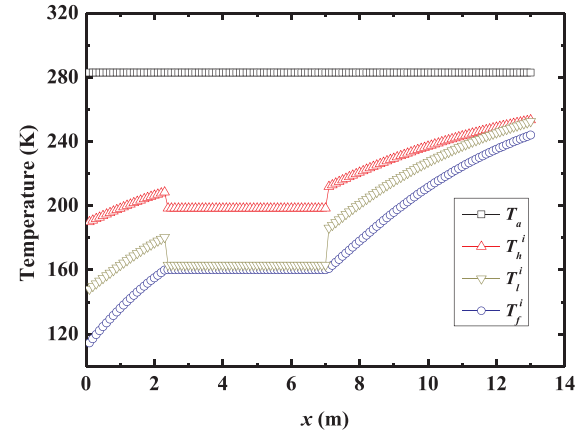

(a) Temperature

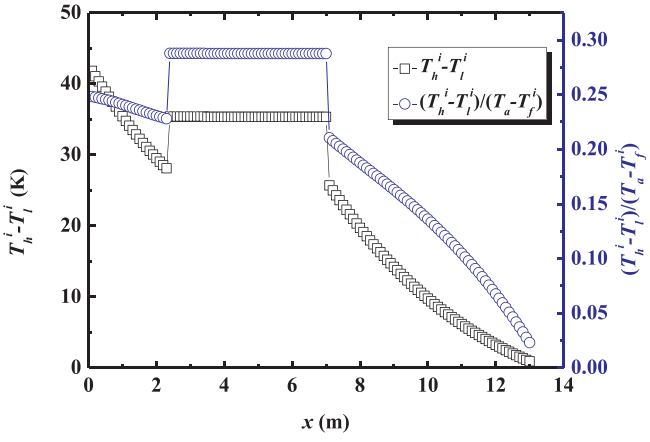

(b) Temperature difference

Fig. 7. Variation of temperature (x-axis).

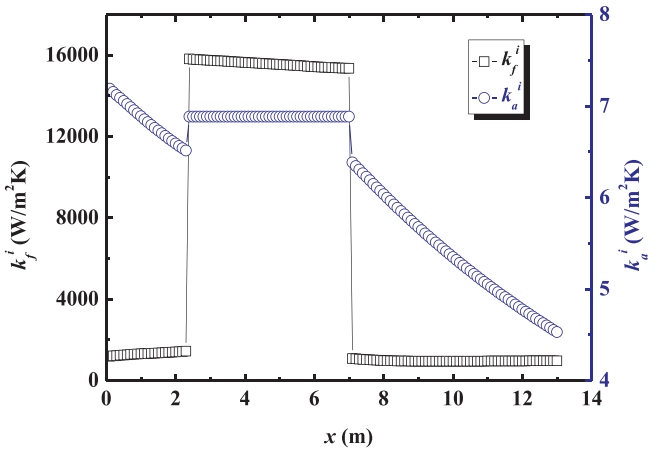

Fig. 8. Variation curves of the heat transfer coefficient in the *x*-direction.

considered to continue heating the LNG to the required temperature. Fig. 9 (b) presents a more intuitive relationship between output power and generation efficiency. For a short tube length, the heat transfer outside the tube was small. Even though the temperature difference between the hot and cold sides of module was large and the generation efficiency was high, the output power was low. With the increase in tube length, the temperature difference between the hot and cold sides of module decreased gradually, and the generation efficiency decreased gradually; however, the heat transfer capacity outside the tube increased, and the output power increased gradually. When the LNG was in the two-phase region, the generation efficiency was high as the LNG temperature remained unchanged, and the output power continued to increase. Thereafter, when the output power reached the maximum value, since the temperature difference between the hot and cold sides of module was small, the voltage generated by the posterior module was not enough to consume itself, resulting in the posterior module becoming a load. The output power of the system decreased, but the generation efficiency decreased gradually as a result of the continuous decrease in the temperature difference between the hot and cold sides. Fig. 9 (c) shows that the variation in the generation density of the VTEG was similar to that of the generation efficiency. When the tube length was less than 6.9 m, the generation density exceeded 21 W/m.

To analyze the abovementioned trends, the distributions of the hot and cold side temperatures of the PN couples along the *x* direction were determined for tube lengths of 2.3 m, 6.9 m, 8.9 m, and 16.6 m. The results are shown in Fig. 10. Under different tube lengths, the temperature of the hot and cold sides changed slightly, and the trends remained quite similar. When $L = 2.2$ m, only the LNG was involved in the generation process. With a gradual decrease in the temperature difference between the hot and cold sides of the PN couples along the *x* direction, the output power decreased gradually along the *x* direction. Hence, there was a gradual increase in the total output power, as shown in Fig. 9 (a), with a decreased amplification. When $L = 6.9$ m, the liquid-phase and two-phase regions in the tube played roles in the generation process. In the two-phase region, because of the slight variations in the hot and cold side temperatures along the *x* direction, the output power and generation efficiency were almost unchanged along the *x* direction, which resulted in an approximately linear increase in the total output power in accordance with an increase in the tube length. When $L = 8.9$ m, a portion of the gaseous natural gas participated in the power generation. With a decrease in the temperature difference between the hot and cold sides of the PN couples in the gas-phase region, the output power decreased along the *x* direction. At this instant, although the rear module exhibited a certain temperature difference, given that the current in all the modules was the same, the generated potential was consumed by the internal resistance of the module. Consequently, the output power was less than or equal to zero.

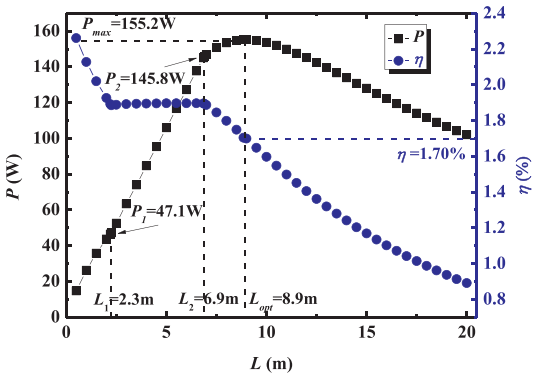

(a) Output power and generation efficiency

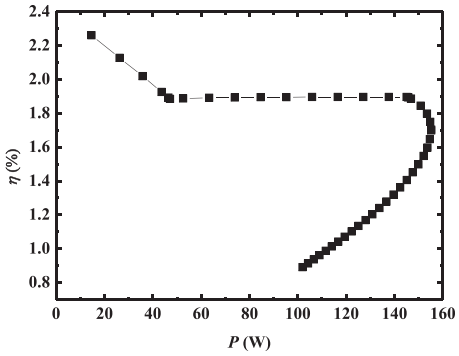

（b）The relationship between generation efficiency and output power

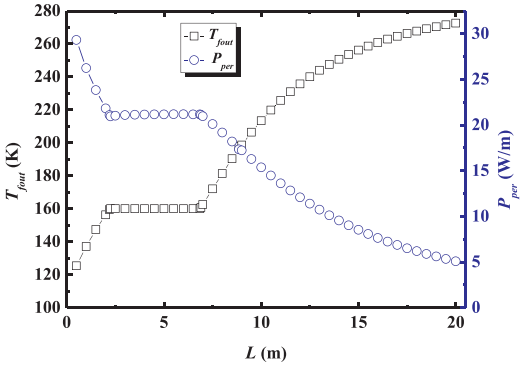

(c) Outlet temperature and generation density

Fig. 9. Effect of tube length on VTEG generation characteristics.

Therefore, an optimal tube length exists for which the VTEG output power is maximum value. Thereafter, further increase in the tube length resulted in a gradual increase in the load module, and the total output power gradually decreased. When $L = 16.6$ m, although the outlet temperature of the natural gas had reached the user requirement, the output power of the rear module was negative, and the cold side temperature of the rear module exceeded the hot side temperature because of the heating of the internal resistance of the module. This indicates that the rear module did not generate further potential, and was completely transformed into a load.

Fig. 11 further presents the variations in power density (*x*-axis) with respect to the tube length. Although the above analysis results indicate that the tube length had a slight influence on the surface temperature of the module, it can be seen from Fig. 11 that changes in the tube length

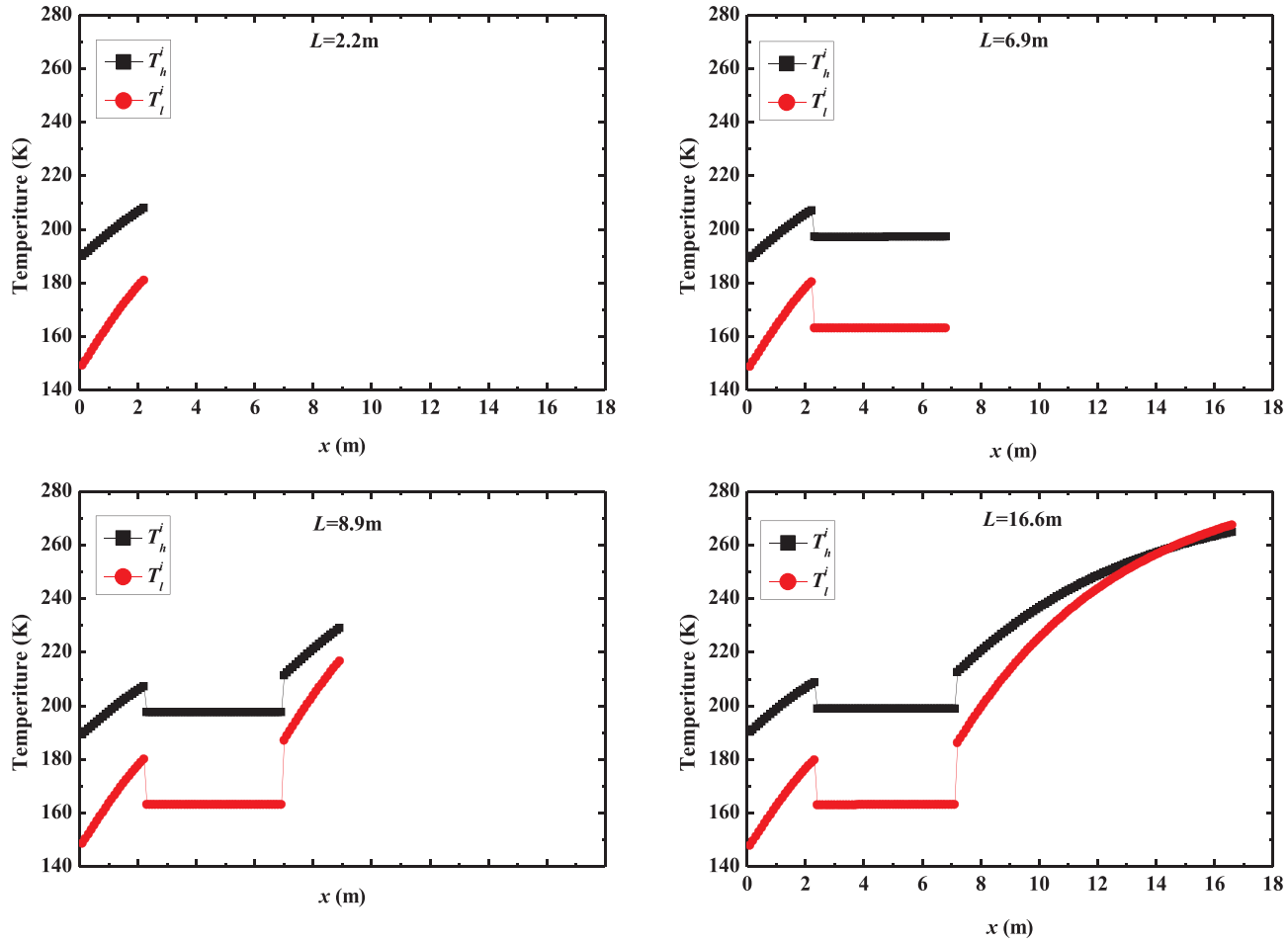

Fig. 10. Variations in temperature (*x*-axis) with respect to tube length.

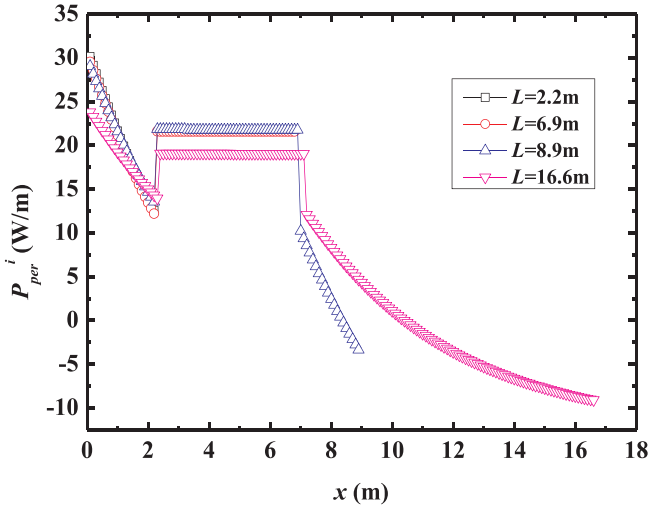

Fig. 11. Variations in power density (*x*-axis) with respect to tube length.

had a more significant influence on the output power of the module (*x*-axis). This is because changes in the tube length were accompanied by changes in the potential generated by the module, and the internal resistance of the entire generator changed, which led to changes in the current flowing through the module. Moreover, the change in current influenced the potential of the module. In summary, the output power varied significantly.

3.3. Influence of flow fluctuation

LNG ambient air vaporizers are widely used in small gasification stations and peak shaving gasification stations. In the actual operation, the LNG flow fluctuates significantly because of changes in the gas consumption of the user. Therefore, this study analyzes the influence of flow on the power generation characteristics of the VTEG. Fig. 12 presents the effect of flow on the power generation characteristics of the VTEG when the tube length is 8.9 m (the optimal tube length under a flow of 100%*U*). As can be seen from Fig. 12 (a), with a decrease in the LNG flow, the hot and cold side temperatures in the liquid-phase and gas-phase regions increased significantly, and no significant changes in the two-phase region were observed. This is because the change in the velocity in the tube had a more significant influence on the single-phase convection region. A decrease in the velocity within the tube resulted in a decrease in the single-phase convection heat transfer coefficient (as shown in Fig. 12 (b)) in addition to an increase in the heat resistance of convective heat transfer, which can raise the inner wall temperature of the tube and increase the hot and cold side temperatures of the PN couples. In the two-phase region, the flow had a slight influence on the boiling heat transfer coefficient; thus, the changes in the hot and cold side temperatures of the module were small.

In addition, it can be seen from Fig. 12 (b) that with a decrease in the flow, the generation density (*x*-axis) decreased significantly. On the one hand, the decrease in flow led to a decrease in the temperature difference between the hot and cold sides of the module, which resulted in a decrease in the open circuit voltage of the module. On the other hand, with a decrease in the flow, the number of modules that transformed into loads increased, thus leading to a reduction in the output

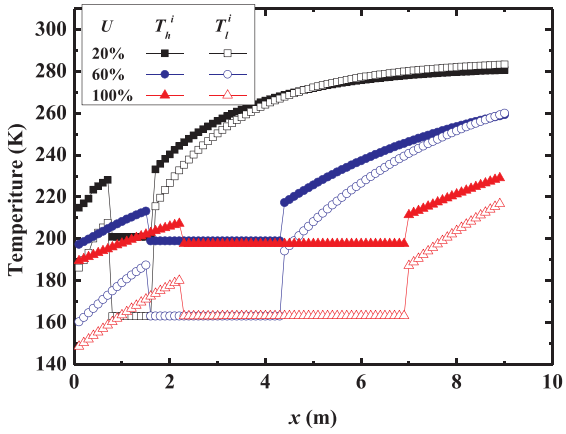

(a) Temperatures of the hot and cold sides

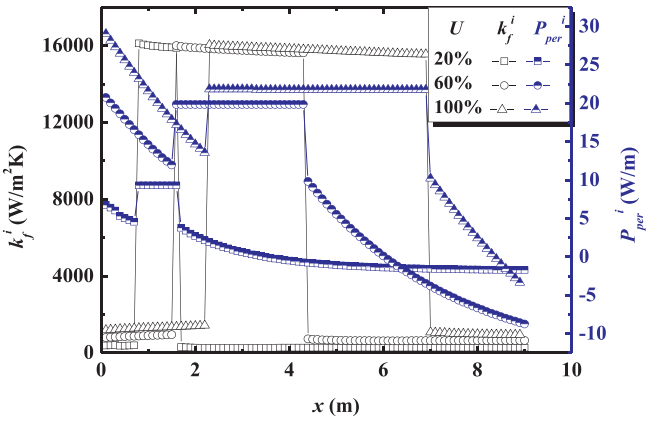

(b) Heat transfer coefficient in the tube and power density

Fig. 12. Variation in main parameters (*x*-axis) with respect to flux (L = 8.9 m).

power on the *x*-axis. Therefore, the influence of the LNG flow on the generation density cannot be neglected.

Fig. 13 further presents the influence of the LNG flow on the performance of the VTEG with respect to the tube length. The output power and generation efficiency exhibited an increasing trend in accordance with an increase in the flow. However, the influence of the flow on the power generation performance varied with respect to the tube length. The variation in the output power and generation efficiency with respect to the flow was smaller when the tube was short. For example, for a tube length of 2 m, when the flow increased from 20% to 90%, the output power increased by 16.4 W, and the generation efficiency increased by 0.50%. However, for a tube length of 8 m, the output power increased by 128.1 W, and the generation efficiency increased by 1.39%. This is because when the tube is short, although the changes in the LNG flow lead to a decrease in the heat transfer coefficient within the tube, the LNG within the tube is constantly in the liquid-phase and two-phase regions (as shown in Fig. 13 (c), the outlet gas temperature is saturated temperature), and a high generation efficiency is maintained. In summary, slight changes in the generation efficiency and output power of the module were observed. However, when the tube was longer, the liquid-phase, two-phase, and gas-phase regions were present in the tube. The increase in the flow increased the heat transfer coefficient within the tube and shortened the length of the gas-phase generation area, which indicates that the number of load modules reduced. Therefore, the increase in the output power and generation efficiency of the VTEG was more significant.

Fig. 14 further presents the optimal tube length and maximum output power for different flows. The optimal tube length and maximum output power increased almost linearly in accordance with an increase in the flow. It is therefore necessary to select a suitable tube length when designing the VTEG. Moreover, a long tube increases the

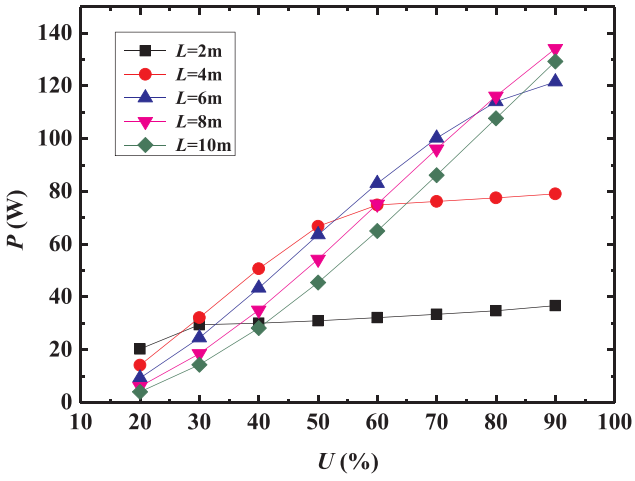

(a) Output power

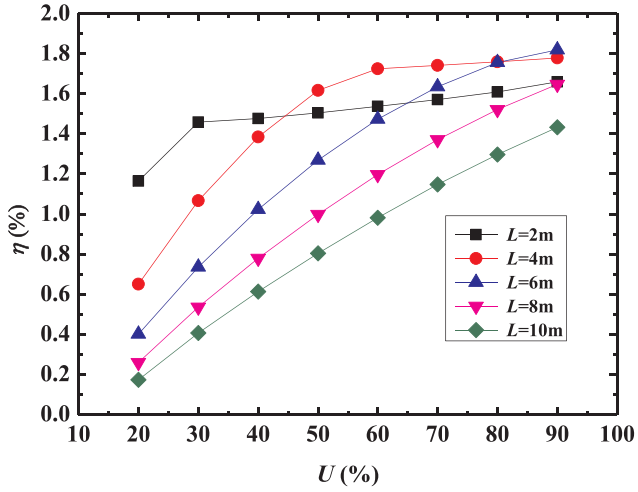

(b) Generation efficiency

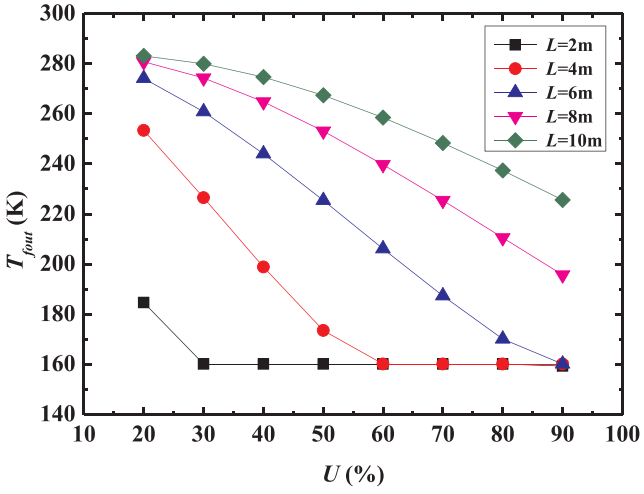

(c) Outlet temperature

Fig. 13. Effect of flow on the performance of the VTEG with respect to the tube length.

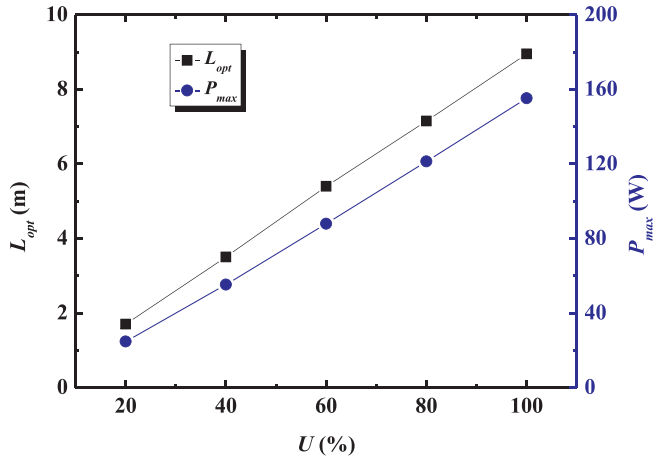

Fig. 14. Optimal tube length and maximum output power with respect to flow.

cost of the system and does not necessarily lead to the maximum output power. If the tube length is excessively short, although a high generation efficiency is maintained, the residual cold energy cannot be effectively utilized when the flow is excessively large. Future work will consider combining the VTEG and traditional vaporizer. The length of the VTEG will be designed according to the commonly used flow, and the residual LNG will be gasified using an auxiliary traditional vaporizer.

3.4. Economic analysis

The operation and maintenance cost of the VTEG can be neglected [50]. Therefore, the primary cost component of the system is the capital investment of the VTEG, and the main revenue is earned from electricity sales. Considering the high cost of thermoelectric materials, the thermoelectric generator module accounts for the biggest expense in VTEG. According to Ref. [51], the cost-effectiveness coefficient (φ) can be used to evaluate the economic performance of the VTEG.

$$\varphi = \frac{P_{\max} t p_e - p_{TE}}{p_{TE}} \tag{30}$$

where P_{max} is the output power, p_e is the price of electricity, t is the life cycle of the module (100,000 h [51]), and p_{TE} is the price of the module US $.

In this study, we considered an output power P_{max} of 155.2 W, corresponding to an optimal tube length of 8.9 m. The relationship between φ and the module price is shown in Fig. 15. It is obvious that the module price for the balance of payments and expenditures increased gradually with the decrease in the price of electricity. When the price of electricity is 0.12 $/kWh, the module price should be less than 12 $/W in order to recover the cost. When the price of electricity is reduced to 0.08 $/kWh, the module price should be less than 8 $/W. As noted in Ref. [52], the current cost of the module is in the range of 5–20 $/W; in the future, this cost may be reduced to 1 $/W. Therefore, in terms of the current price of the commercial module, the VTEG can obtain considerable benefits by choosing the cost-effective module.

Fig. 16 presents the variation in the payback period of the VTEG for different prices of electricity at different module prices. It can be seen that with the decrease of module price and increase of electricity price, the payback period of the investment decreases significantly. Taking the price of electricity as 0.08 $/kWh for example, when the module price reaches 5 $/W, the payback period of the investment is 62,500 h, whereas the value is only 12,500 h when the module price reduces to 1 $/W. This means that the development of high performance thermoelectric modules is of great significance for LNG cold energy thermoelectric generation.

Compared to power cycle generation technology, VTEG does not have superior generation efficiency. Taking the two-stage condensation combined cycle for LNG cold energy [12] as an example, the generation efficiency can be calculated to reach 12.17%, whereas the value of LNG cold energy thermoelectric generation may only be 1.70%. It is obvious that the generation efficiency of the VTEG is far lower than that of power cycle generation. However, from the economic point of view, owing to the complexity of equipment, the economic advantage of power cycle generation is not obvious. For example, as noted in Ref. [53], the generation cost of the single-stage condensation Rankine cycle is 0.664 $/W, whereas the current generation cost of the VTEG is approximately 5–20 $/W. Therefore, VTEG is expected to perform better economically. Considering that the simple structure, no mechanical moving parts, no working medium, safe and reliable operation, and convenient maintenance of thermoelectric generation are not available in other power generation technologies. Moreover, it has good adaptability to the flow fluctuations of LNG. Therefore, it can be widely used in various places for LNG gasification. In addition, further development of high-efficiency and low-temperature thermoelectric materials, and optimization of the structural parameters of the generator can also improve the generation efficiency of the VTEG. Thus, LNG cold energy thermoelectric generation is expectable.

4. Conclusions

The gasification process of LNG releases a significant amount of cold energy. In this paper, a novel type of vaporizer is proposed by combining an air-heated vaporizer with a thermoelectric generator. The proposed vaporizer combines the LNG gasification process with the thermoelectric generation process for the recovery of LNG cold energy for power generation. Based on the established model, the power generation characteristics were analyzed. The main conclusions of this study are as follows:

(1) Compared with the traditional vaporizer, the outer wall temperature of the VTEG is higher for the same tube length, which mitigates the frosting problem on the vaporizer surface. The generation area of the VTEG is divided into the liquid-phase, two-phase, and gas-phase regions. In the single-phase region, the generation efficiency and density gradually decreased along the flow direction of the LNG, whereas in the two-phase region, the generation efficiency and density were maintained at approximately 1.91% and 20.8 W/m, respectively. In addition, the results revealed that the low heat transfer coefficient outside the tube was the main reason for the lower generation efficiency of the VTEG. The generation performance can be further improved by optimizing the external structure

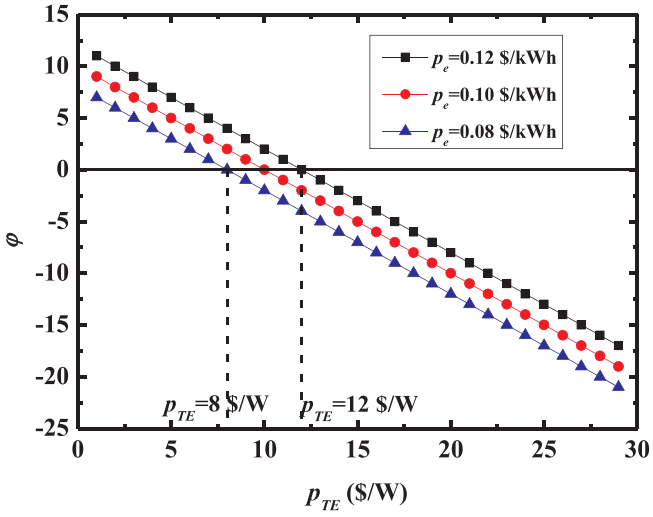

Fig. 15. Economic analysis of the VTEG.

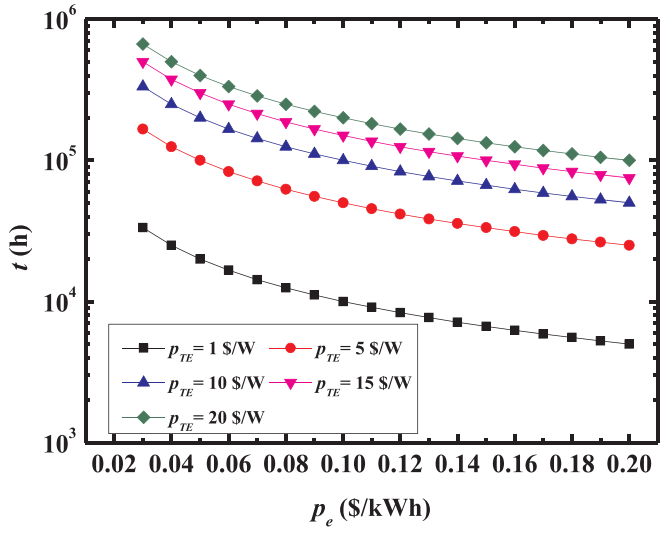

Fig. 16. Variation in the payback period with price of electricity for different module prices.

parameters or applying to the seawater vaporizer.

(2) An increase in the VTEG tube length resulted in an initial increase in the output power, followed by a decrease, whereas the generation efficiency initially decreased, became constant, and was then followed by a rapid decrease. An optimal tube length was found to exist, at which the VTEG output power was maximum, but the outlet temperature of LNG cannot meet the user requirements. The traditional vaporizer can thus be considered to complete the subsequent gasification.

(3) The variations in flow had a more significant influence on the heat transfer coefficient and the hot and cold side temperatures of the PN couples in the single-phase region. With a constant tube length, the output power and generation efficiency increased in accordance with an increase in the flow. However, when the tube length was short, the influence of the flow on the generation performance was relatively small. In addition, the optimal tube length and maximum output power increased linearly in accordance with an increase in the flow. In future work, the VTEG tube length will be designed according to the common flow.

Declaration of Competing Interest

The authors declare that they have no known competing financial interests or personal relationships that could have appeared to influence the work reported in this paper.

Acknowledgments

The authors are grateful for the National Key Research and Development Program of China (2017YFE0198000), the Natural Science Foundation of China (51906056), the Natural Science Foundation of Hebei Province (E2018202158) and the Open Fund Program of the Key Laboratory of Efficient Utilization of Low and Medium Grade Energy (Tianjin University), Ministry of Education of China (201907-303).

References

[1] Kumar S, Kwon HT, Choi KH, Lim W, Cho JH, Tak K, et al. LNG: an eco-friendly cryogenic fuel for sustainable development. Appl Energy 2011;88:4267–73.
[2] Kanbur BB, Xiang L, Dubey S, Choo FH, Duan F. Cold utilization systems of LNG: a review. Renew Sustain Energy Rev 2017;79:1171–88.
[3] Liu HT, You L. Characteristics and applications of the cold heat exergy of liquefied natural gas. Energy Convers Manage 1999;40:1515–25.
[4] Gao T, Lin W, Gu A. Improved processes of light hydrocarbon separation from LNG with its cryogenic energy utilized. Energy Convers Manage 2011;52:2401–4.
[5] Xu S, Cheng Q, Zhuang L, Tang B, Ren Q, Zhang X. LNG vaporizers using various refrigerants as intermediate fluid: Comparison of the required heat transfer area. J Nat Gas Sci Eng 2015;25:1–9.
[6] Liu S, Jiao W, Wang H. Three-dimensional numerical analysis of the coupled heat transfer performance of LNG ambient air vaporizer. Renew Energy 2016;87:1105–12.
[7] Jin T, Wang M, Tang K. Simulation and performance analysis of a heat transfer tube in SuperORV. Cryogenics 2014;61:127–32.
[8] Xu W, Duan J, Mao W. Process study and exergy analysis of a novel air separation process cooled by LNG cold energy. J Therm Sci 2014;23:77–84.
[9] Messineo A, Panno D. Potential applications using LNG cold energy in Sicily. Int J Energy Res 2008;32:1058–64.
[10] Zhang N, Lior N. A novel near-zero CO2 emission thermal cycle with LNG cryogenic exergy utilization. Energy 2006;31:1666–79.
[11] Cao W, Beggs C, Mujtaba IM. Theoretical approach of freeze seawater desalination on flake ice maker utilizing LNG cold energy. Desalination 2015;355:22–32.
[12] Bao J, Lin Y, Zhang R, Zhang X, Zhang N, He G. Performance enhancement of two-stage condensation combined cycle for LNG cold energy recovery using zeotropic mixtures. Energy 2018;157:588–98.
[13] Shi XS, Che D. A combined power cycle utilizing low-temperature waste heat and LNG cold energy. Energy Convers Manage 2009;50:567–75.
[14] García RF, Carril JC, Gomez JR, Gomez MR. Power plant based on three series Rankine cycles combined with a direct expander using LNG cold as heat sink. Energy Convers Manage 2015;101:285–94.
[15] Franco A, Casarosa C. Thermodynamic analysis of direct expansion configurations for electricity production by LNG cold energy recovery. Appl Therm Eng 2015;78:649–57.
[16] Deng SM, Jin HG, Cai RX, Lin RM. Novel cogeneration power system with liquefied natural gas(LNG) cryogenic exergy utilization. Energy 2004;29:497–512.
[17] Wang JF, Yan ZQ, Wang M, Dai YP. Thermodynamic analysis and optimization of an ammonia-water power system with LNG(liquefied natural gas) as its heat sink. Energy 2013;50:513–22.
[18] Dong H, Zhao L, Zhang S, Wang A, Cai J. Using cryogenic exergy of liquefied natural gas for electricity production with the Stirling cycle. Energy 2013;63:10–8.
[19] Champier D. Thermoelectric generators: A review of applications. Energy Convers Manage 2017;140:167–81.
[20] Meng JH, Wang XD, Chen WH. Performance investigation and design optimization of a thermoelectric generator applied in automobile exhaust waste heat recovery. Energy Convers Manage 2016;120:71–80.
[21] Su S, Liu T, Wang Y, Chen X, Wang J, Chen J. Performance optimization analyses and parametric design criteria of a dye-sensitized solar cell thermoelectric hybrid device. Appl Energy 2014;120:16–22.
[22] Zhao Y, Wang S, Ge M, Liang Z, Liang Y, Li Y. Performance analysis of automobile exhaust thermoelectric generator system with media fluid. Energy Convers Manage 2018;171:427–37.
[23] Kim TY, Kwak J, King B. Energy harvesting performance of hexagonal shaped thermoelectric generator for passenger vehicle applications: An experimental approach. Energy Convers Manage 2018;160:14–21.
[24] Zhao Y, Wang S, Ge M, Liang Z, Liang Y, Li Y. Performance investigation of an intermediate fluid thermoelectric generator for automobile exhaust waste heat recovery. Appl Energy 2019;239:425–33.
[25] Yin E, Li Q, Xuan Y. Thermal resistance analysis and optimization of photovoltaic thermoelectric hybrid system. Energy Convers Manage 2017;143:188–202.
[26] Ge M, Wang Z, Liu L, Zhao J, Zhao Y. Performance analysis of a solar thermoelectric generation (STEG) system with spray cooling. Energy Convers Manage 2018;177:661–70.
[27] Liu H, Meng J, Wang X, Chen W. A new design of solar thermoelectric generator with combination of segmented materials and asymmetrical legs. Energy Convers Manage 2018;175:11–20.
[28] Zhao Y, Wang S, Ge M, Li Y, Liang Z. Analysis of thermoelectric generation characteristics of flue gas waste heat from natural gas boiler. Energy Convers Manage 2017;148:820–9.
[29] Gholamian E, Habibollahzade A, Zare V. Development and multi-objective optimization of geothermal-based organic Rankine cycle integrated with thermoelectric generator and proton exchange membrane electrolyzer for power and hydrogen production. Energy Convers Manage 2018;174:112–25.
[30] Apertet Y, Ouerdane H, Goupil C, Lecoeur P. Equivalent parameters for series thermoelectric. Energy Convers Manage 2015;93:160–5.
[31] Apertet Y, Ouerdane H. Small-signal model for frequency analysis of thermoelectric systems. Energy Convers Manage 2017;149:564–9.
[32] Ouerdane H, Apertet Y, Goupil C, Lecoeur P. Continuity and boundary conditions in thermodynamics: From Carnot's efficiency to efficiencies at maximum power. Eur Phys J-Spec Top 2015;224(5):839–64.
[33] Shen ZG, Wu SY, Xiao L. Assessment of the performance of annular thermoelectric couples under constant heat flux condition. Energy Convers Manage 2017;150:704–13.
[34] Sun W, Hu P, Chen Z, et al. Performance of cryogenic thermoelectric generators in LNG cold energy utilization. Energy Convers Manage 2005;46:789–96.
[35] Karabetoglu S, Sisman A, Ozturk ZF, Sahin T. Characterization of a thermoelectric generator at low temperatures. Energy Convers Manage 2012;62:47–50.
[36] Chung D-Y, Hogan T, Brazis P, et al. CsBi4Te6: A High-Performance Thermoelectric Material fot Low-Temperature Applications. Science 2000;287:1024–7.
[37] Kambe M, Morita R, Omoto K, Koji Y, Yoshida T, Noishiki K. Thermoelectric Module Performance in Cryogenic Temperature. Journal of Power and Energy Systems

2010;4(1):12–26.
[38] Kambe M, Morita R, Omoto K, Koji Y, Yoshida T, Noishiki K. Thermoelectric Power Conversion System Combined with LNG Vaporizer. Journal of Power and Energy Systems 2008;2(6):1304–19.
[39] Jeong ES. Optimization of power generating thermoelectric modules utilizing LNG cold energy. Cryogenics 2017;88:29–35.
[40] Fan S, Gao Y. Numerical simulation on thermoelectric and mechanical performance of annular thermoelectric generator. Energy 2018;150:38–48.
[41] Yang S, Tao W. Heat transfer. 3rd ed. Beijing: Higher Education Press; 2004.
[42] Fang X, Xu Y, Zhou Z. New correlations of single-phase friction factor for turbulent pipe flow and evaluation of existing single-phase friction factor correlations. Nucl Eng Des 2011;241:897–902.
[43] Zou X, Gong MQ, Chen GF, et al. Experimental study on saturated flow boiling heat transfer of R170/R290 mixtures in a horizontal tube. Int J Refrig 2010;33(2):371–80.
[44] Shen ZG, Wu SY, Xiao L. Theoretical analysis on the performance of annular thermoelectric couple. Energy Convers Manage 2015;89:244–50.
[45] Yang C, Jiao W, Yang G, Zhao Y, Ma J. Calculation of Heat Transfer in LNG Ambient Air Vaporizer. Gas & Heat 2012;32(7):B12–7.
[46] Zhang AB, Wang BL, Pang DD, He LW, Lou J, Wang J, et al. Effects of interface layers on the performance of annular thermoelectric generators. Energy 2018;147:612–20.
[47] Niu X, Yu J, Wang S. Experimental study on low-temperature waste heat thermoelectric generator. J Power Sources 2009;188:621–6.
[48] Zhao Y, Wang S, Ge M, Li Y, Yang Y. Energy and exergy analysis of thermoelectric generator system with humidifiedflue gas. Energy Convers Manage 2018;156:140–9.
[49] Liu S, Jiao W, Ren L, Wang H, Zhang P. Dynamic heat transfer analysis of liquefied natural gas ambient air vaporizer under frost conditions. Appl Therm Eng 2017;110:999–1006.
[50] Khanmohammadi S, Saadat-Targhi M. Thermodynamic and economic assessment of an integrated thermoelectric generator and the liquefied natural gas production process. Energy Convers Manage 2019;185:603–10.
[51] Su H, Zhou F, Qi H, Li J. Design for thermoelectric power generation using subsurface coal fires. Energy 2017;140:929–40.
[52] Siddique ARM, Mahmud S, Van Heyst B. A review of the state of the science on wearable thermoelectric power generators (TEGs) and their existing challenges. Renew Sustain Energy Rev 2017;73:730–44.
[53] Bao J, Yuan T, Zhang L, Zhang N, Zhang X, He G. Comparative study of liquefied natural gas (LNG) cold energy power generation systems in series and parallel. Energy Convers Manage 2019;184:107–26.